DOI: 10.1002/cphc.201000884

High-Performance Oxygen Sensors Based on Eu^{III} Complex/Polystyrene Composite Nanofibrous Membranes Prepared by Electrospinning

Yinghui Wang,[a, b] Bin Li,*[a] Liming Zhang,[a] Qinghui Zuo,[a, b] Peng Li,[a, b] Jun Zhang,[c] and Zhongmin Su*[c]

An optical oxygen sensor based on an Eu^{III} complex/polystyrene (PS) composite nanofibrous membrane is prepared by electrospinning. The emission intensity of [$Eu(TTA)_3$(phencarz)] (TTA = 2-thenoyltrifluoroacetonate, phencarz = 2-(*N*-ethylcarbazolyl-4)imidazo[4,5-*f*]1,10-phenanthroline) decreases with increasing oxygen concentration, and thus the [$Eu(TTA)_3$(phencarz)]/PS composite nanofibrous membranes can be used as an optical oxygen-sensing material based on emission quenching caused by oxygen. Elemental analysis, UV/Vis absorption spectra, scanning electron microscopy (SEM), fluorescence microscopy, luminescence-intensity quenching Stern–Volmer plots, and excited-state decay analysis are used to characterize the obtained oxygen-sensing materials. A high sensitivity (I_{N2}/I_{O2}) of 3.38 and short response and recovery times ($t_{\downarrow} = 5.0$, $t_{\uparrow} = 8.0$ s) are obtained. These results are the best values reported for oxygen sensors based on Eu^{III} complexes. The high surface area-to-volume ratio and porous structure of the electrospun nanofibrous membranes are taken to be responsible for the outstanding performance.

1. Introduction

Determination of molecular-oxygen concentration in both gas and liquid phases is a very important issue in different fields such as oceanography, meteorology, biology, environmental science, and life science.[1] Recently, optical oxygen sensors have attracted considerable interest because they are inexpensive, easy to miniaturize, simple to use, not easily poisoned, respond quickly, and do not consume oxygen, in contrast to conventional electrochemical methods.[1a] Such sensors are based upon the principle that oxygen is a powerful quencher of the electronic excited states of luminescent complexes. Among the widely investigated luminescent dyes for oxygen-sensing purposes, luminescent transition metal complexes, such as those of Pt^{II},[2] Ru^{II},[3] Au^{I},[4] and Re^{I},[5] have been frequently employed in a number of oxygen-sensing systems. Eu^{III} complexes are well known for their excellent luminescence properties, for example, extremely sharp emission peaks, long lifetimes, and strong luminescence with high quantum efficiencies, which well meet the requirements for oxygen-sensing materials. Nevertheless, only a few reports have appeared describing the sensitivity of emission intensity and lifetime of Eu^{III} complexes to oxygen.[6] Amao and co-workers successfully developed Eu^{III} complexes as oxygen-sensing materials by incorporating them into continuous polymer films. However, the obtained sensitivities are not satisfactory (not more than 2.0) to meet actual applications. In fact, not all Eu^{III} complexes are perturbed in their luminescence by variations in oxygen concentration. Only when the energy gap between the $^5D_0$ level of the Eu^{3+} ion and the triplet energy of the ligand is less than 1500 cm^{-1} is the luminescence of Eu^{III} complexes sensitive to the presence of oxygen.[7] Therefore, a promising way to improve the sensitivity of Eu^{III} complexes is to modulate the triplet energy of the ligand. For practical applications in optical oxygen-sensing devices, it is necessary to incorporate these luminescent complexes into a solid matrix serving as a support for the complexes and allowing oxygen transport from the surroundings. The support may have to meet quite stringent criteria for suitable performance. For example, a high diffusion coefficient is necessary for a rapid response, and effective local quenching around oxygen probes is necessary for good sensitivity.

Polymers are reported to be ideal supports for dyes in optical chemical sensors owing to their good mechanical strength and thermal stability. Among the numerous polymers, polystyrene (PS) is an excellent candidate as sensor matrix owing to its good processability. Many luminescent transition metal complexes have been incorporated into PS continuous thin films, and applications in optical oxygen sensors have also been demonstrated.[8] However, the oxygen diffusion coeffi-

[a] *Dr. Y. Wang, Prof. B. Li, L. Zhang, Q. Zuo, P. Li*
Key Laboratory of Excited State Processes
Changchun Institute of Optics, Fine Mechanics and Physics
Chinese Academy of Sciences
Changchun, 130033 (P. R. China)
Fax: (+86) 431-86176935
E-mail: lib020@yahoo.cn

[b] *Dr. Y. Wang, Q. Zuo, P. Li*
Graduate School of the Chinese Academy of Sciences
Chinese Academy of Sciences, Beijing, 100039 (P. R. China)

[c] *Dr. J. Zhang, Prof. Z. Su*
Department of Chemistry, Northeast Normal University
Changchun 130024 (P. R. China)
E-mail: zmsu@nenu.edu.cn

Supporting information for this article is available on the WWW under http://dx.doi.org/10.1002/cphc.201000884.

cient of continuous polymer thin film is not high enough, resulting in long response time and nonlinear Stern–Volmer quenching curve. Recently, it was demonstrated that nanofibrous membranes prepared by electrospinning are excellent host materials for developing functional materials because of their large surface area-to-volume ratio, unique nanoscale architecture, simple and cost-effective preparation method, as well as potential applications in nanodevices.[9] We prepared the first optical oxygen sensor based on a Cu^{I} complex by using electrospun nanofibrous polymer membranes as matrix.[10] The outstanding performance and simple and versatile preparation method make the obtained nanofibrous membranes promising candidates as matrices for optical oxygen sensors. However, up to now, there is no report on the oxygen-sensing properties of Eu^{III} complex/polymer nanofibrous membranes prepared by electrospinning.

We have now incorporated an Eu^{III} complex [$Eu(TTA)_3$(phencarz)] (TTA = 2-thenoyltrifluoroacetonate, phencarz = 2-(*N*-ethylcarbazolyl-4)imidazo[4,5-*f*]-1,10-phenanthroline; Figure 1)

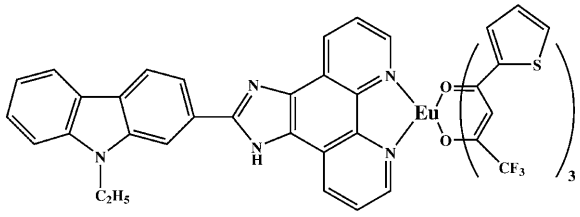

Figure 1. Molecular structure of [$Eu(TTA)_3$(phencarz)].

into composite nanofibrous PS membranes by electrospinning. The optical oxygen-sensing properties of [$Eu(TTA)_3$(phencarz)]/PS composite nanofibrous membranes were investigated on the basis of luminescence intensity quenching. Changes in sensitivity, Stern–Volmer plots, and excited-state decays of all samples were also studied. For the composite nanofibrous membranes with optimum content of 3 wt% [$Eu(TTA)_3$(phencarz)] relative to PS, high sensitivity (I_{N2}/I_{O2}) of 3.38 and short response/recovery times ($t_{\downarrow}$ = 5.0, $t_{\uparrow}$ = 8.0 s) were obtained. These are the best values reported for oxygen sensors based on Eu^{III} complexes.

2. Results and Discussion

2.1. Morphology

[$Eu(TTA)_3$(phencarz)]/PS composite nanofibers were prepared by electrospinning solutions of [$Eu(TTA)_3$(phencarz)]/PS in DMF. In the following, [$Eu(TTA)_3$(phencarz)]/PS composite nanofibrous membranes electrospun from 1, 2, 3, and 4 wt% concentrations of [$Eu(TTA)_3$(phencarz)] relative to PS in DMF solution are labeled as samples A, B, C, and D, respectively. An SEM image and a fluorescence micrograph of sample C are shown in Figure 2. The electrospun nanofibers are randomly oriented on the substrate without any evidence of bead-on-string morphology, and their average diameter is 400–500 nm. The fluorescence micrograph of sample C shows bright red emission of [$Eu(TTA)_3$(phencarz)], which confirms that [$Eu(TTA)_3$(phencarz)] was successfully electrospun into composite nanofibrous membranes.

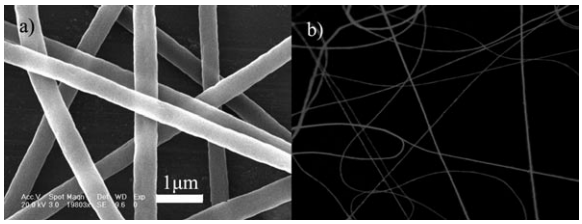

Figure 2. a) SEM image and b) fluorescence micrograph of sample C.

2.2. Photophysical Properties

The UV/Vis absorption spectra of [$Eu(TTA)_3$(phencarz)] and the free ligand phencarz in CH_2Cl_2 solution and those of [$Eu(TTA)_3$(phencarz)], PS, and samples A–D in the solid state are presented in Figure 3. As for [$Eu(TTA)_3$(phencarz)] in CH_2Cl_2 solution,

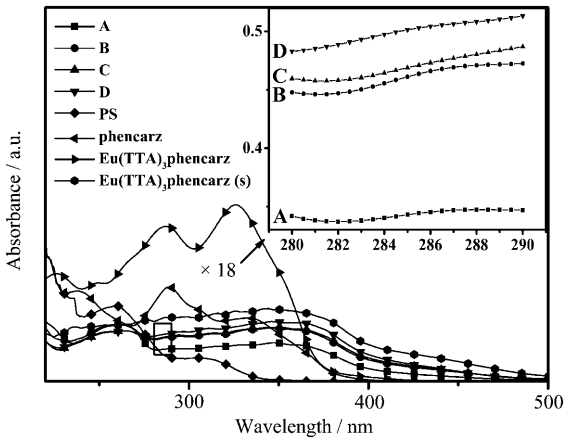

Figure 3. UV/Vis absorption spectra of [$Eu(TTA)_3$(phencarz)] and ligand phencarz in CH_2Cl_2 solution and those of [$Eu(TTA)_3$(phencarz)], PS, and samples A–D in the solid state.

the absorption bands located around 226, 287, and 326 nm are attributed to π–π* electronic transitions of phencarz by comparison to the absorption spectrum of phencarz. Moreover, we find a blueshift of the major electronic transitions (238→226, 289→287, 333→326 nm) between ligand phencarz and [$Eu(TTA)_3$(phencarz)], which may be attributed to the coordinative interaction between the Eu^{3+} ion and phencarz, which raises the energy levels of the major π–π* transition and thus results in an obvious blueshift.[11] In contrast to the absorption spectrum of [$Eu(TTA)_3$(phencarz)] in CH_2Cl_2 solution, its solid-state absorption spectrum shows broadening and a progressive redshift, that is the solvent influences its absorption. Two absorption bands are located around 258 and 309 nm in pure PS fibers. All of the aforesaid absorption bands are found in the spectra of samples A–D, and this is further proof that we

have successfully incorporated [Eu(TTA)$_3$(phencarz)] into a PS matrix.

The emission spectra of [Eu(TTA)$_3$(phencarz)] under nitrogen, air, and oxygen atmospheres (Figure 4) show characteristic emission lines of the Eu^{3+} ion, which are assigned to the transitions $^5D_0$–$^7F_0$ (578 nm), $^5D_0$–$^7F_1$ (591 nm), $^5D_0$–$^7F_2$ (610 nm), $^5D_0$–$^7F_3$ (650 nm), and $^5D_0$–$^7F_4$ (700 nm). The significant dependence of the emission intensity of [Eu(TTA)$_3$(phencarz)] on the concentration of oxygen indicates that the complex probably has oxygen-sensing properties.

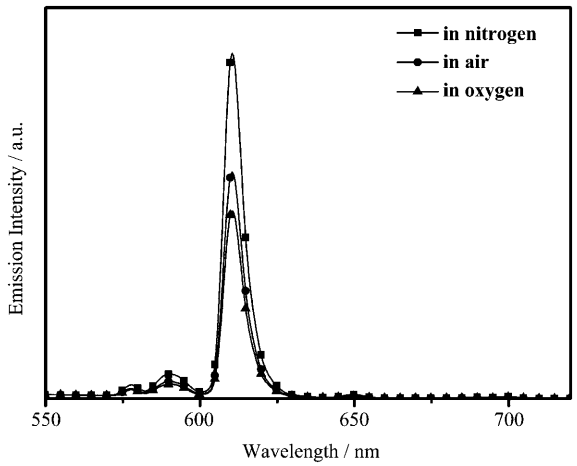

Figure 4. Emission spectra of [Eu(TTA)$_3$(phencarz)] under nitrogen, air, and oxygen (λ_{ex} = 378 nm).

2.3. Oxygen-Sensing Properties

To test the oxygen-sensing performance of the [Eu(TTA)$_3$(phencarz)]/PS composite nanofibrous membranes, emission spectra of samples A–D under different oxygen concentrations were recorded at room temperature (see Figure S1 in the Supporting Information). The $^5D_0$–$^7F_2$ emission peak of Eu^{3+} ion is located at 610 nm and maintains a constant position at different oxygen concentrations. However, the relative intensity decreased markedly with increasing oxygen concentration. The relative luminescent intensities of samples A–D decrease by 50.2, 62.8, 70.3, and 62.0%, respectively, on changing from pure nitrogen to pure oxygen. Sample C exhibits the highest sensitivity of the four samples. We ascribe this result to the different quantum efficiencies of the four samples. Quantum efficiencies of the four samples were calculated according to the literature[12] to be 0.24, 0.29, 0.31, and 0.28, respectively, which is consistent with the trend of the sensitivity. When the doping concentration is low (1 and 2 wt%), the quantum efficiency of the [Eu(TTA)$_3$(phencarz)]/PS composite nanofibrous membrane is comparatively low, which results in low sensitivity; when it is too high (4 wt%), intermolecular interaction between probe molecules may become serious, resulting in low quantum efficiency and sensitivity. Thus, 3 wt% [Eu(TTA)$_3$(phencarz)] relative to PS is the optimum level, leading to high quantum efficiency and sensitivity.

Generally, the luminescence of most lanthanide complexes is not perturbed by variations of oxygen concentration. For Eu^{III} complexes ($^5D_0$ Eu at 17200 cm^{-1}), if the triplet energy of ligand is higher than 22000 cm^{-1}, the luminescence of the Eu^{3+} ion is generally not sensitive to the presence of oxygen.[7] However, when the energy gap between the two states is less than 1500 cm^{-1}, competitive thermally activated energy backtransfer will occur and the luminescence of the Eu^{3+} ion will become sensitive to the presence of oxygen.[13] The mechanism is depicted in Scheme 1. In fact, molecular oxygen does not quench the Eu^{3+} ion excited state, but relates to the quenching of the intermediate triplet state of the antenna ligand and affects the Eu^{3+} ion luminescence. When the energy gap between the $^5D_0$ level of Eu^{3+} ion and the triplet energy of ligand is less than 1500 cm^{-1}, thermally activated energy backtransfer can occur rapidly at ambient temperature, which lengthens the lifetime of the aromatic triplet state.[13c] At the same time, this renders the triplet state of the ligand susceptible to dynamic quenching by atmospheric oxygen.

To demonstrate the energy-transfer process of [Eu(TTA)$_3$(phencarz)], the phosphorescence spectra of [Gd(phencarz)$_2$Cl$_3$] and [Gd(TTA)$_3$(H$_2$O)$_2$] were measured at 77 K to give data on the triplet energy levels of the corresponding ligands (Figure 5). From the phosphorescence spectra, the triplet energy levels of [Gd(phencarz)$_2$Cl$_3$] and [Gd(TTA)$_3$(H$_2$O)$_2$] were determined from the corresponding shortest-wavelength phosphorescence band to be 2.22 eV (558 nm) and 2.33 eV (532 nm), respectively. Because the Gd^{3+} ion does not have energy levels in the visible part of the electromagnetic spectrum, the data obtained from the phosphorescence spectra actually reveal the triplet energy levels of phencarz and TTA in Eu^{III} complexes. The singlet-state energy levels of phencarz and TTA were estimated by referencing their absorbance edges, which are 3.18 eV (390 nm) and 3.08 eV (402 nm), respectively. The singlet- and triplet-state energy levels are illustrated in Figure 6. For [Eu(TTA)$_3$(phencarz)], as the energy gap between the $^5D_0$ level of the Eu^{3+} ion and triplet energy of the ligand is 721 cm^{-1}, reverse energy transfer occurred, resulting in effective luminescence quenching by molecular oxygen. Thus, the energy-transfer process further confirmed the oxygen-sensing

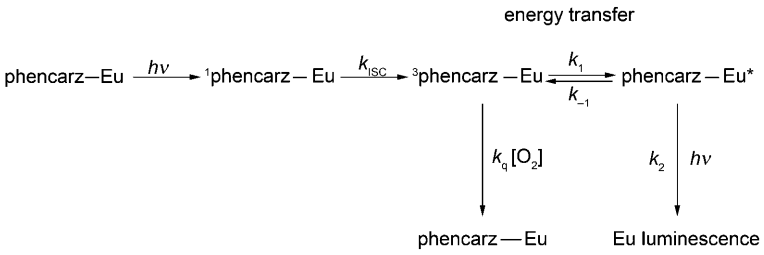

Scheme 1. Kinetic scheme of the luminescence of [Eu(TTA)$_3$(phencarz)] quenched by oxygen molecules.

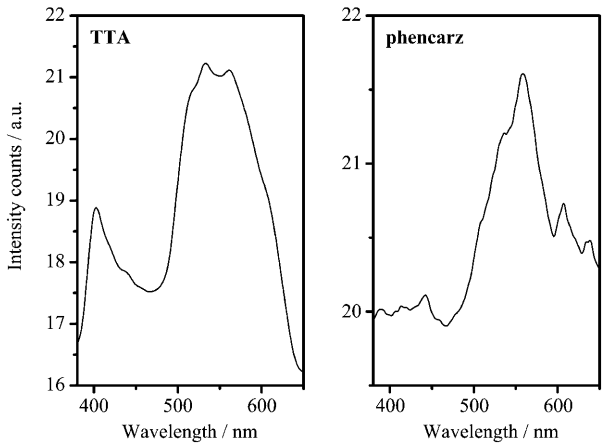

Figure 5. Phosphorescence spectrum of $[Gd(phencarz)_2Cl_3]$ and $[Gd(TTA)_3(H_2O)_2]$ at 77 K ($\lambda_{ex} = 355$ nm).

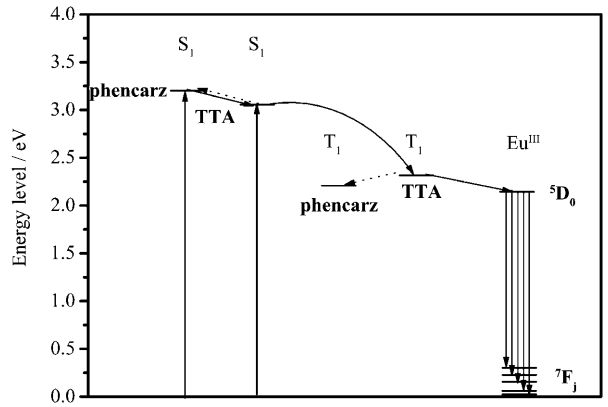

Figure 6. Schematic energy-level diagram and energy-transfer process. S_1: first excited singlet state; T_1: first excited triplet state.

mechanism of $[Eu(TTA)_3(phencarz)]$/PS composite nanofibrous membranes.

Oxygen quenching is diffusion-limited and can be described by the Stern–Volmer relationship in a homogeneous microenvironment [Eq. (1)]:[14]

$$I_0/I = 1 + K_{SV}[O_2] = 1 + k_q\tau_0[O_2] \quad (1)$$

where I is the steady-state luminescence intensity of the luminophore, the subscript 0 denotes the absence of oxygen, τ_0 is the excited-state luminescence lifetime in the absence of oxygen, K_{SV} the Stern–Volmer constant, k_q the bimolecular rate constant describing the efficiency of the collisional encounters between the luminophore and the quencher, and $[O_2]$ the oxygen concentration. For this ideal case, a plot of I_0/I versus $[O_2]$ will be linear with a slope equal to K_{SV} and an intercept of unity, which allows a simple single-point sensor calibration. The lifetime decay of the luminophore in homogeneous media can be described by a single-exponential equation [Eq. (2)]:[15]

$$I(t) = \alpha \exp(-t/\tau) \quad (2)$$

where $I(t)$ is the luminescence intensity at time t, and α the preexponential factor. However, nonlinear Stern–Volmer plots are often obtained when quenching takes place in a solid matrix. The deviation from linearity is attributed to the simultaneous presence of static and dynamic quenching, and the heterogeneity of the microenvironment of the immobilized luminophore molecules in the matrix.[8f,16] It is believed that the luminophore molecules are distributed simultaneously between two or more sites within the matrix, one of which is more heavily quenched than the others. Consequently, the Equation (1) used in the ideal homogeneous environment is not suitable for these nonlinear Stern–Volmer plots. Several models have been proposed to explain deviation from linearity.[3b,15a,17] Among them, the two-site Demas model has been proved to have excellent ability to fit the experimental data in heterogeneous solid-based systems. The intensity Stern–Volmer equation becomes Equation (3):

$$\frac{I_0}{I} = \frac{1}{\frac{f_{01}}{1+K_{SV1}[O_2]} + \frac{f_{02}}{1+K_{SV2}[O_2]}} \quad (3)$$

where f_{0i} is the steady-state fraction of light emitted from the ith site and K_{SVi} is its Stern–Volmer constant. The Stern–Volmer plots of samples A–D over the full oxygen concentration range studied (0–100% O_2) are shown in Figure 7, and they are best

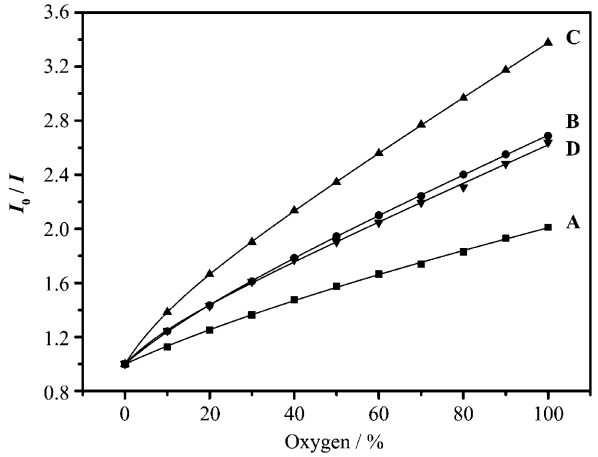

Figure 7. Stern–Volmer plot for all samples under different oxygen concentrations.

fitted by using the two-site Equation (3). The best-fitting parameters are compiled in Table 1. Inspection of these results reveals that $[Eu(TTA)_3(phencarz)]$ molecules are distributed heterogeneously in the PS matrix. They mainly occupy two distinctly different environments: one is readily accessible to oxygen, and the other less accessible. Although the two-site model for the luminophore within the polymer layer is far from describing the real situation,[18] the data we obtained are best fitted by using two-site Equation (3), and the square regression factor r^2 of all the samples are near 0.9999. Therefore, we speculate that $[Eu(TTA)_3(phencarz)]$ molecules are distribut-

Table 1. Oxygen-sensing properties of the [Eu(TTA)$_3$(phencarz)]/PS composite nanofibrous membranes.

Sample	I_{N2}/I_{O2}	$t_\uparrow$ [s]	$t_\downarrow$ [s]	Demas two-site model[a]			
				K_{SV1} [(% O_2)$^{-1}$]	K_{SV2} [(% O_2)$^{-1}$]	f_{01}	r^2
A	2.01	11.3	7.0	0.0221 ± 0.0054	0.00034 ± 0.0019	0.60 ± 0.17	0.9996
B	2.69	8.7	4.7	0.0508 ± 0.0054	0.0088 ± 0.0007	0.44 ± 0.05	0.9999
C	3.38	8.0	5.0	0.0508 ± 0.0054	0.1010 ± 0.0047	0.57 ± 0.01	0.9999
D	2.64	8.3	5.0	0.0104 ± 0.0012	0.0929 ± 0.0394	0.72 ± 0.08	0.9994

[a] Terms are from [Eq (3)]. $f_{01}+f_{02}=1$.

ed over *i* sites in the PS composite nanofibrous membrane, but mainly in two sites, which means that the date can be fitted well by using the two-sites model. Sample C shows the highest sensitivity and K_{SV} values among the four samples, which indicates that [Eu(TTA)$_3$(phencarz)] molecules in sample C are more easily quenched by oxygen. This further confirms that the sample doped with 3 wt% of [Eu(TTA)$_3$(phencarz)] has the optimum level.

In Demas two-site models, there are two excited-state lifetime components for the luminescence species, and the excited lifetime decay analysis can be described by Equation (4):

$$I(t) = \alpha_1 \exp(-t/\tau_1) + \alpha_2 \exp(-t/\tau_2) \quad (4)$$

where *I*(t) is the fluorescence intensity at time *t*, the subscripts 1 and 2 denote the assigned lifetime components, and α_i denotes the pre-exponential factors. The weighted mean lifetime τ_m can be calculated by Equation (5):[3a]

$$\langle \tau_m \rangle = \sum_{i=1}^{2} \alpha_i \tau_i \Big/ \sum_{i=1}^{2} \alpha_i \quad (5)$$

Figure 8 shows the time-resolved intensity-decay curves of samples A–D measured in the presence of pure N_2, and their fitting parameters are summarized in Table 2. The results clearly show that the time-resolved intensity decays of [Eu(TTA)$_3$(phencarz)]/PS composite nanofibrous membranes are at least

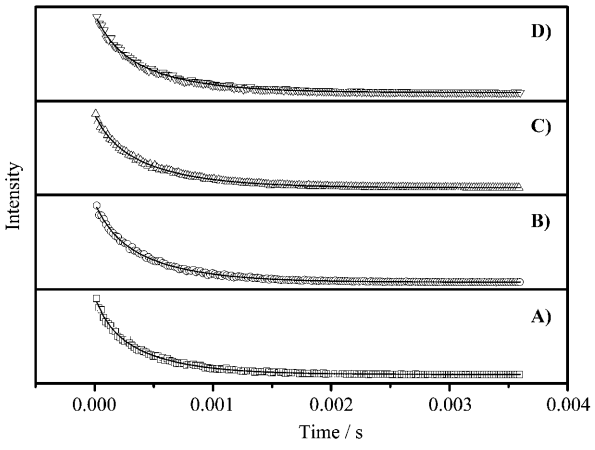

Figure 8. Time-resolved intensity-decay curve of all samples in the absence of oxygen (pure N_2). Fit to a two-exponential decay model is shown (solid lines).

double-exponential. This is a common behavior for a luminophore doped in a wide variety of host matrixes.[17d–e,19] The result of the time-resolved decay curves is consistent with the Stern–Volmer plots (Figure 7), that is, [Eu(TTA)$_3$(phencarz)] is mainly distributed between two

Table 2. Excited-state lifetime decay constants of [Eu(TTA)$_3$(phencarz)]/PS composite nanofibrous membranes.

Sample	α_1	τ_1 [ms]	α_2	τ_2 [ms]	$\langle\tau\rangle$[a] [ms]	r^2
A	0.03	0.47	0.01	0.12	0.36	0.9980
B	0.01	0.14	0.03	0.52	0.41	0.9983
C	0.07	0.53	0.02	0.13	0.43	0.9989
D	0.01	0.15	0.03	0.51	0.40	0.9980

[a] Lifetime measurements were performed under unquenched conditions (N_2) and calculated by Equation (5).

sites in the PS matrix, one of which is more heavily quenched than the other. Moreover, the excited-state lifetime of sample C is slightly longer than those of other three samples, which is consistent with the varying tendencies of sensitivity, quantum efficiency, and K_{SV}. All of these data demonstrate that the optimum doping level is 3 wt% [Eu(TTA)$_3$(phencarz)] relative to PS.

The oxygen-sensing properties of all samples are summarized in Table 1. A sensor with I_{N2}/I_{O2} greater than 3.0 is a suitable oxygen-sensing device.[3] The I_{N2}/I_{O2} value of sample C is 3.38, which to the best of our knowledge is the highest value for optical oxygen sensors based on Eu^{III} complexes that has been achieved until now. We attribute the excellent performance to three reasons. Firstly, since the triplet-state energy level of ligand phencarz is close to that of the $^5D_0$ level of the Eu^{3+} ion, reverse energy transfer can occur easily, and effective quenching of luminescence by molecular oxygen results. Secondly, PS is an excellent host material owing to its good processability, which ensured that it could be electrospun into a porous membrane. Finally, the porous structure of the electrospun membrane not only provides a large surface area-to-volume ratio but also facilitates entry and diffusion of oxygen, which is the most important reason.

For an oxygen sensor, short response and recovery times are very important factors in evaluating its feasibility of practical application. Figure 9 shows the typical dynamic response of all the samples on exposure to alternating pure N_2 and O_2 atmospheres. Generally, 95% response time, that is, $t_\downarrow$(95%, $N_2 \rightarrow O_2$), is defined as the time required for the luminescent intensity to decrease by 95% on changing from 100% N_2 to 100% O_2. Similarly, 95% recovery time, that is, $t_\uparrow$(95%, $O_2 \rightarrow N_2$), is the time required for the luminescence intensity to reach the 95% of its initial value recorded under 100% N_2 on changing from 100% O_2 to 100% N_2. The response time $t_\downarrow$ and recovery time $t_\uparrow$ of sample C are 5.0 and 8.0 s, respectively. To the best of our knowledge, these are the shortest response and recovery

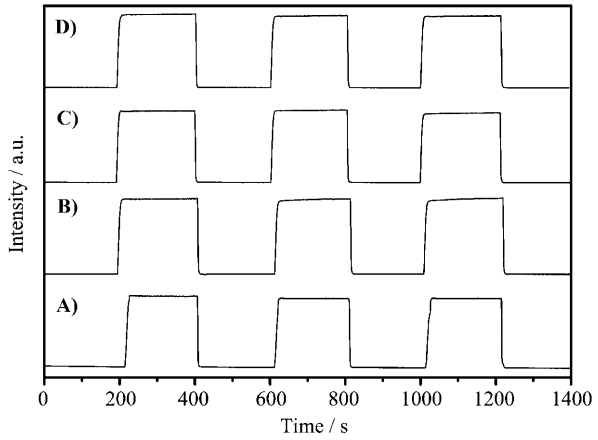

Figure 9. Response time and relative intensity change of all samples exposed to alternating environments of 100% nitrogen and 100% oxygen.

times for oxygen sensors based on Eu^{III} complexes. We ascribe the fast response and recovery to the fact that the porous structure of the electrospun membranes facilitates diffusion of oxygen.

3. Conclusions

Optical oxygen sensors based on [$Eu(TTA)_3$(phencarz)]/PS composite nanofibrous membranes were prepared by electrospinning. The sensitivity of up to 3.38 indicates that they are highly sensitive to oxygen. These materials showed good linearity according to the Demas two-site model (sites more and less accessible to oxygen) for Stern–Volmer plots versus O_2 concentration, and have good operational stability and reproducibility and short response and recovery times. The excellent performance can be explained by the following three facts: 1) since the energy difference between the triplet-state energy level of phencarz and the $^5D_0$ level of Eu^{3+} ion is only 721 cm^{-1}, reverse energy transfer can occur easily, and effective luminescence quenching by molecular oxygen results; 2) the porous structure of the electrospun membrane with large surface area-to-volume favors oxygen diffusion; 3) PS is an excellent host material owing to its good processability, which ensured that it could be electrospun into porous membrane. The good performances and the simple and versatile preparation method indicate that composite nanofibrous membranes containg Eu^{III} complexes have potential applications in the field of oxygen sensors.

Experimental Section

Materials: 2-Thenoyltrifluoroacetone (HTTA) was purchased from Aldrich Chemical Company. Eu_2O_3 (99.99%) and NaOH (AR) were purchased from Sinopharm Chemical Reagent Company. $EuCl_3$ was prepared by dissolving Eu_2O_3 in concentrated hydrochloric acid. All reagents and chemicals were used without further purification.

Characterization: Elemental analyses were carried out on a Vario Element Analyzer. The UV/Vis absorption spectra were obtained on a UV/Vis spectrophotometer (Shimadzu, UV-3100). A field emission scanning electron microscope (FESEM, XL30, FEI) and fluorescence microscope (BX51T-3200, Olympus) were used to observe the morphologies of nanofibers. Phosphorescence spectra were measured in dichloromethane by using an Edinburgh FLS 920 fluorescence spectrophotometer at 77 K with cooling by liquid nitrogen and excitation at 355 nm.

The oxygen-sensing properties based on luminescence intensity quenching of the obtained samples were characterized by using a Hitachi-4500 fluorescence spectrophotometer equipped with a xenon lamp (150 W) operating in the 200–900 nm range. The emission spectra of different samples were obtained under excitation at 378 nm. For the Stern–Volmer plots, oxygen and nitrogen were mixed at different concentrations via gas flow controllers and flowed directly into the gas chamber sealed with a close-fitting Suba-Seal rubber lid equipped with inlet and outlet tubes. We typically allowed 1 min between changes in N_2/O_2 concentrations to ensure that a new equilibrium point had been established. Equilibrium was evident when the luminescence intensity remained constant ($\pm$2%). The sensing response curves were obtained with the same instruments.

The time-resolved intensity decay measurements were carried out by using a Nd:YAG laser system (Spectra Physics). The linewidth, repetition frequency, and pulse duration of the laser light were 1 cm^{-1}, 10 Hz, and 10 ns, respectively. Owing to interference from the excitation source, geometrical considerations resulted in a sample orientation of 90° to prevent reflected and scattered excitation from entering the detector. N_2 gas was delivered to the sealed gas chamber in exactly the same manner as described above for the Stern–Volmer measurements. The maximum emission was set at 610 nm, and the luminescence generated was detected with a photomultiplier. The signal was relayed through a 50$\times$ termination plug and passed to a digital phosphor oscilloscope (Tektronix, Beaverton, Oregon, US; Model TDS 3052), which was used to resolve the lifetime decay curves. All reported measured lifetimes were averaged 2400 times. The electronic excited-state decay time profiles were subsequently stored and analyzed by using Origin 7.5. The emission lifetimes were obtained from biexponential curve fittings, and the mean values for the two emission lifetime components and the corresponding pre-exponentially weighted emission lifetimes are reported throughout. All measurements were performed at ambient temperature (23$\pm$5 °C).

Synthesis of [$Eu(TTA)_3$(phencarz)]: Phencarz was synthesized according to literature procedures,[20] and [$Eu(TTA)_3$(phencarz)] according to the conventional method with minor modifications.[21] HTTA (0.067 g, 0.3 mmol) and phencarz (0.041 g, 0.1 mmol) were dissolved in ethanol (5 mL) under stirring. Sodium hydroxide was added until the pH value of the solution approached 7. Then $EuCl_3 \cdot 6H_2O$ (0.037 g, 0.1 mmol) in water (2 mL) was added to the mixed solution. The mixture was stirred for 1 h at 60 °C. The product was collected by filtration and recrystallized from ethanol. Elemental analysis (%) calcd for $C_{51}H_{31}N_5F_9O_6S_3Eu$: C 49.84, H 2.54, N 5.70; found: C 49.68, H 2.51, N 5.74.

Synthesis of [$Gd(phencarz)_2Cl_3$]: $GdCl_3 \cdot 6H_2O$ (1 mmol) in water (0.1 mL) was added dropwise under stirring to a solution of phencarz (2 mmol) in ethanol (50 mL), and the solution was heated to reflux for 2 h. The resulting solution was filtered and a white yellow powder was obtained.

Synthesis of [$Gd(TTA)_3(H_2O)_2$]: HTTA (3.0 mmol) was dissolved in ethanol (50 mL). NaOH (3.0 mL, 1.0 mol L^{-1}) was then added dropwise, and the mixture was stirred for 15 min. Then $GdCl_3 \cdot 6H_2O$ (1 mmol) in water (0.1 mL) was added dropwise under stirring and

the solution was heated to reflux for 2 h. A yellow powder was obtained by precipitation from ethanol/water solution.

Preparation of Electrospun Composite Nanofibrous Membranes: An appropriate amount of PS ($M_w = 100\,000$) was dissolved in DMF at a concentration of 22 wt% at room temperature. After vigorous stirring, different amounts of [Eu(TTA)$_3$(phencarz)] (1, 2, 3, and 4 wt% relative to PS, samples A–D, respectively) were added to the solution. Then the solution was put into a glass syringe and electrospun by applying 16 kV at an electrode distance of 16 cm. The fibers were collected on an aluminum frame.

Acknowledgements

The authors gratefully acknowledge the financial support of the National Natural Science Foundations of China (Grant No. 50872130) and the Science and Technology Developing Project of Jinlin Province (Grant No. 20100533).

Keywords: electrospinning · lanthanides · luminescence · membranes · sensors

[1] a) Y. Amao, *Microchim. Acta* **2003**, *143*, 1–12; b) B. T. Glazer, A. G. Marsh, K. Stierhoff, G. W. Luther, *Anal. Chim. Acta* **2004**, *518*, 93–100; c) H. Hasumoto, T. Imazu, T. Miura, K. Kogure, *J. Oceanogr.* **2006**, *62*, 99–103; d) Y. Amao, T. Miyashita, I. Okura, *Anal. Chim. Acta* **2000**, *421*, 167–174; e) K. Mitsubayashi, Y. Wakabayashi, D. Murotomi, T. Yamada, T. Kawase, S. Iwagaki, I. Karube, *Sens. Actuators B* **2003**, *95*, 373–377.

[2] C. Huo, H. D. Zhang, H. Y. Zhang, H. Y. Zhang, B. Yang, P. Zhang, Y. Wang, *Inorg. Chem.* **2006**, *45*, 4735–4742.

[3] a) B. Lei, B. Li, H. Zhang, Sh. Lu, Z. Zheng, W. Li, Y. Wang, *Adv. Funct. Mater.* **2006**, *16*, 1883–1891; b) K. A. McGee, D. J. Veltkamp, B. J. Marquardt, K. R. Mann, *J. Am. Chem. Soc.* **2007**, *129*, 15092–15093; c) R. Q. Albuquerque, Z. Popović, L. De Cola, G. Calzaferri, *ChemPhysChem* **2006**, *7*, 1050–1053.

[4] A. Mills, A. Lepre, B. R. C. Theobald, E. Slade, B. A. Murrer, *Anal. Chem.* **1997**, *69*, 2842–2847.

[5] L. Huynh, Z. Wang, J. Yang, V. Stoeva, A. Lough, I. Manners, M. A. Winnik, *Chem. Mater.* **2005**, *17*, 4765–4773.

[6] a) Y. Amao, I. Okura, T. Miyashita, *Chem. Lett.* **2000**, 934–935; b) Y. Amao, I. Okura, T. Miyashita, *Bull. Chem. Soc. Jpn.* **2000**, *73*, 2663–2668; c) Y. Amao, I. Okura, T. Miyashita, *Chem. Lett.* **2000**, 1286–1287.

[7] G. L. Law, R. Pal, L. O. Palsson, D. Parker, K. L. Wong, *Chem. Commun.* **2009**, 7321–7323.

[8] a) Y. Cai, A. Smith, J. Shinar, R. Shinar, *Sens. Actuators B* **2010**, *146*, 14–22; b) Z. Zhou, R. Shinar, A. J. Allison, J. Shinar, *Adv. Funct. Mater.* **2007**, *17*, 3530–3537; c) V. I. Ogurtsov, D. B. Papkovsky, *Sens. Actuators B* **2006**, *113*, 917–929; d) Y. Amao, K, Asai, I. Okura, *J. Porphyrins Phthalocyanines* **2000**, *4*, 292–299; e) S. J. Payne, G. L. Fiore, C. L. Fraser, J. N. Demas, *Anal. Chem.* **2010**, *82*, 917–921; f) P. Hartmann, M. J. P. Leiner, M. E. Lippitsch, *Anal. Chem.* **1995**, *67*, 88–93; g) J. F. Fernández-Sánchez, T. Roth, R. Cannas, Md. K. Nazeeruddin, S. Spichiger, M. Graetzel, U. E. Spichiger-Keller, *Talanta* **2007**, *71*, 242–250; h) M. C. DeRosa, P. J. Mosher, G. P. A. Yap, K.-S. Focsaneanu, R. J. Crutchley, C. E. B. Evans, *Inorg. Chem.* **2003**, *42*, 4864–4872; i) M. T. Miller, T. B. Karpishin, *Sens. Actuators B* **1999**, *61*, 222–224.

[9] a) J. Yoon, S. K. Cha, J. M. Kim, *J. Am. Chem. Soc.* **2007**, *129*, 3038–3039; b) J. Jang, J. Ha, J. Cho, *Adv. Mater.* **2007**, *19*, 1772–1775; c) S. K. Chae, H. Park, J. Yoon, C. H. Lee, D. J. Ahn, J. M. Kim, *Adv. Mater.* **2007**, *19*, 521–524; d) D. Li, Y. N. Xia, *Adv. Mater.* **2004**, *16*, 1151–1170.

[10] Y. H. Wang, B. Li, Y. H. Liu, L. M. Zhang, Q. H. Zuo, L. F. Shi, Z. M. Su, *Chem. Commun.* **2009**, 5868–5870.

[11] J. L. Liu, B. Yan, *J. Phys. Chem. B* **2008**, *112*, 10898–10907.

[12] a) Y. Li, B. Yan, H. Yang, *J. Phys. Chem. C* **2008**, *112*, 3959–3968; b) X. Guo, H. Guo, L. Fu, R. Deng, W. Chen, J. Feng, S. Dang, H. Zhang, *J. Phys. Chem. C* **2009**, *113*, 2603–2610.

[13] a) N. Sabbatini, M. Guardigli, J. M. Lehn, *Coord. Chem. Rev.* **1993**, *123*, 201–228; b) D. Parker, J. A. G. Williams, *J. Chem. Soc. Dalton Trans.* **1996**, 3613–3628; c) A. Beeby, D. Parker, J. A. G. Williams, *J. Chem. Soc. Perkin Trans. 2* **1996**, 1565–1579.

[14] C. Malins, S. Fanni, H. G. Glever, J. G. Vos, B. D. MacCraith, *Anal. Commun.* **1999**, *36*, 3–4.

[15] a) E. R. Carraway, J. N. Demas, B. A. DeGraff, J. R. Bacon, *Anal. Chem.* **1991**, *63*, 337–342; b) M. T. Murtagh, M. R. Shahriari, M. Krihak, *Chem. Mater.* **1998**, *10*, 3862–3869.

[16] M. E. Lippitsch, S. Draxler, *Sens. Actuators B* **1993**, *11*, 97–101.

[17] a) J. R. Bacon, J. N. Demas, *Anal. Chem.* **1987**, *59*, 2780–2785; b) W. Y. Xu, R. C. McDonough, B. Langsdorf, J. N. Demas, B. A. DeGraff, *Anal. Chem.* **1994**, *66*, 4133–4141; c) S. Draxler, M. E. Lippitsch, I. Klimant, M. Kraus, O. S. Wolfbeis, *J. Phys. Chem.* **1995**, *99*, 3162–3167; d) J. N. Demas, B. A. Deora, W. Y. Xu, *Anal. Chem.* **1995**, *67*, 1377–1380; e) L. A. Sacksteder, J. N. Demas, B. A. DeGraffIt, *Anal. Chem.* **1993**, *65*, 3480–3483.

[18] a) J. López-Gejo, D. Haigh, G. Orellana, *Langmuir* **2010**, *26*, 2144–2150; b) K. Eaton, B. Douglas, P. Douglas, *Sens. Actuators B* **2004**, *97*, 2–12.

[19] a) B. H. Han, I. Manners, M. A. Winnik, *Chem. Mater.* **2005**, *17*, 3160–3171; b) Y. Tang, E. C. Tehan, Z. Tao, F. V. Bright, *Anal. Chem.* **2003**, *75*, 2407–2413.

[20] H. Xin, F. Y. Li, M. Guan, C. H. Huang, M. Sun, K. Z. Wang, Y. A. Zhang, L. P. Jin, *J. Appl. Phys.* **2003**, *94*, 4729–4731.

[21] H. Bauer, J. Blanc, D. L. Ross, *J. Am. Chem. Soc.* **1964**, *86*, 5125–5131.

Received: October 21, 2010
Published online on January 11, 2011

